

# In Vivo Biodistribution, PET Imaging, and Tumor Accumulation of $^{86}\text{Y}$ - and $^{111}\text{In}$ -Antimindin/RG-1, Engineered Antibody Fragments in LNCaP Tumor-Bearing Nude Mice

Douglas W. Schneider<sup>1</sup>, Tara Heitner<sup>2</sup>, Bruno Alicke<sup>3</sup>, David R. Light<sup>2</sup>, Kirk McLean<sup>2</sup>, Noboru Satozawa<sup>2</sup>, Gordon Parry<sup>1</sup>, Jeongsoo Yoo<sup>4</sup>, Jason S. Lewis<sup>4</sup>, and Renate Parry<sup>1</sup>

<sup>1</sup>Cancer Research, Berlex Biosciences/Schering AG, Richmond, California; <sup>2</sup>Antibody Technology, Berlex Biosciences/Schering AG, Richmond, California; <sup>3</sup>Pharmacology, Berlex Biosciences/Schering AG, Richmond, California; and <sup>4</sup>Mallinckrodt Institute of Radiology, Washington University School of Medicine, St. Louis, Missouri

To optimize in vivo tissue uptake kinetics and clearance of engineered monoclonal antibody (mAb) fragments for radiotherapeutic and radiodiagnostic applications, we compared the biodistribution and tumor localization of four  $^{111}\text{In}$ - and  $^{86}\text{Y}$ -labeled antibody formats, derived from a single antimindin/RG-1 mAb, in a prostate tumor model. The IgG, diabody, single-chain variable domain (scFv), and novel miniantibody formats, composed of the human IgE-C<sub>H4</sub> and a modified IgG1 hinge linked to scFv domains, were compared. **Methods:** Antibodies were first derivatized with the bifunctional chelator CHX-A''-diethylenetriamine pentaacetic acid and then bound to the radiometal to create radiolabeled immunoconjugates. Human LNCaP xenografts were grown in nude mice, and  $^{111}\text{In}$ - or  $^{86}\text{Y}$ -labeled antibodies were administered intravenously. Tissues were harvested at different times, and the level of antibody deposition was determined by measuring radioactivity. Whole-body small-animal PET of mice receiving  $^{86}\text{Y}$ -labeled antibodies was performed at 6 time points and colocalized with simultaneous micro-CT imaging. **Results:** The biodistributions of  $^{111}\text{In}$  and  $^{86}\text{Y}$  antibodies were quite similar. The blood, tumor, kidney, and liver tissues contained varying levels of radioactivity. The antibody accumulation in the tumor correlated with molecular size. The IgG steadily increased with time to 24.1 percentage injected dose per gram (%ID/g) at 48 h. The miniantibody accumulated at a similar rate to reach a lower level (14.2 %ID/g) at 48 h but with a higher tumor-to-blood ratio than the IgG. Tumor accumulation of the diabody peaked at 3 h, reaching a much lower level (3.7 %ID/g). A combination of rapid clearance and lower relative affinity of the scFv precluded deposition in the tumor. Small-animal PET results correlated well with the biodistribution results, with similar tumor localization patterns. **Conclusion:** The larger antibody formats (IgG and miniantibody) gave higher tumor uptake levels than did the smaller formats (diabody and scFv). These larger formats may

be more suitable for radioimmunotherapy applications, evidenced by the preclinical efficacy previously shown by a report on the IgG format. The smaller formats were rapidly cleared from circulation, and the diabody, which accumulated in the tumor, may be more suitable for radiodiagnostic applications.

**Key Words:**  $^{86}\text{Y}$  PET;  $^{111}\text{In}$  biodistribution; mindin; RG-1; IgE-C<sub>H4</sub> miniantibody

**J Nucl Med 2009; 50:435–443**

DOI: 10.2967/jnumed.108.055608

**M**onoclonal antibodies (mAbs) as radioimmunotherapeutic and radiodiagnostic imaging agents for cancer continue to have great potential. The use of a single antibody format for both imaging and therapeutic applications would be advantageous. However, requirements for therapeutic agents (compared with those for diagnostic agents)—such as in vivo clearance rate, radiologic half-life, tissue uptake, energy emission, and tissue penetration—differ, presenting technical challenges.

The human mindin homolog, mindin/RG-1, is a member of the mindin/F-spondin family of extracellular matrix proteins (1) and is expressed in normal human prostate and prostate tumor tissues, including androgen-independent tissue and metastases to lymph node and bone (2). The human antimindin/RG-1 mAb (19G9) IgG is a promising format for PET imaging in mindin/RG-1-expressing tumor xenografts in mice, after conjugation with [(R)-2-amino-3-(4-isothiocyanatophenyl) propyl]-*trans*-(S,S)-cyclohexane-1,2-diamine-pentaacetic acid (CHX-A''-DTPA) and  $^{86}\text{Y}$  labeling (2). This conjugate is efficacious in radioimmunotherapy in the same tumor model after  $^{90}\text{Y}$  labeling. This study clearly showed the potential for the powerful combination of  $^{86}\text{Y}$  imaging for accurate dosimetry calculations

Received Jul. 1, 2008; revision accepted Nov. 24, 2008.

For correspondence or reprints contact: Douglas W. Schneider, Molecular and Antibody Biology, Bayer Healthcare Pharmaceuticals, 2600 Hilltop Dr., Richmond, CA 94804.

E-mail: doug.schneider@bayer.com

COPYRIGHT © 2009 by the Society of Nuclear Medicine, Inc.

with  $^{90}\text{Y}$  therapy using the same 19G9 IgG antibody–chelator format. Theoretically, however, the identical antibody formats may not be optimal for both diagnostic and therapeutic applications targeting tumors, unless dosimetry measurements are applied before therapy with the  $^{90}\text{Y}$  construct. Diagnostic applications generally require tumor deposition combined with rapid blood clearance and minimal accumulation in nontumor tissues. Therapeutic applications often require longer circulation times while minimizing radiologic toxicity to normal tissues by reducing nontumor tissue accumulation. The kinetics of in vivo biodistribution and clearance will depend on the antibody format used and may differ between antibody conjugates used for imaging the tumor or those used to kill tumor cells. In this study, we compare the biodistribution and PET properties of 4 matched antibody formats of the 19G9 antibody. All are potent binders of mindin/RG-1 after conjugation by CHX-A''-DTPA and labeling with either  $^{111}\text{In}$  or  $^{86}\text{Y}$ . The antibody formats used in this study (Fig. 1) vary in molecular size: IgG (150 kDa), the novel huIgE-C<sub>H</sub>4 mini-antibody (85 kDa) (3–5), the divalent single-chain variable domain (scFv) or “diabody” (50 kDa) (3), and the monovalent scFv (25 kDa) (6). This study compares biodistribution kinetics and PET of 4 antibody formats derived from the same mAb using the same antibody–chelator conjugate.

## MATERIALS AND METHODS

### Construction of Monomer and Dimer Single-Chain Formats of 19G9 Antibody

The mammalian cell expression vector pIE (Medarex), previously described to express 19G9 IgG antibody (2), was used to construct a bacterial vector for expression of the single-chain antibody 19G9 scFv by published methods (7). The resultant 19G9 scFv construct was then used to create a second bacterial vector to

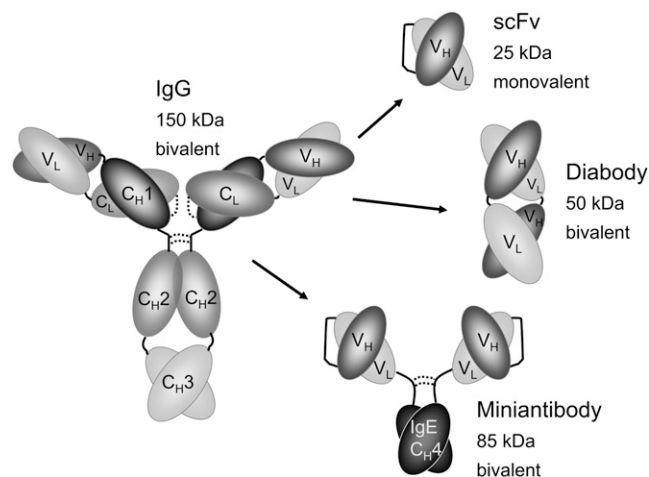


**FIGURE 1.** Schematic representation of mAb 19G9 (IgG) and antibody fragment formats (scFv, diabody, and IgE-C<sub>H</sub>4 mini-antibody) showing different Ig domains (solid lines indicate hinges, linkers, and loops; dashed lines indicate interdomain disulfides).

express the 19G9 diabody (dimeric single-chain antibody) and a mammalian vector to express the 19G9 miniantibody expression vector. DNA coding the variable heavy (V<sub>H</sub>) and variable light (V<sub>L</sub>) chains from maxipreps (Qiagen) of pIE were amplified by polymerase chain reaction (PCR) using primers introducing restriction sites and sites for overlap extension, creating the 20–amino acid linker between V<sub>H</sub> and V<sub>L</sub> of the scFv (GlyGlyGlyGlySer)<sub>4</sub>. After 15 cycles of extension, the scFv was amplified with the forward and back primers (V<sub>H</sub> forward primer: *GCGGCCAGCCGGC-CATGGCCAGGTTTCAGCTGGTGC AGTC*; V<sub>H</sub> back primer: *CCACCGGAGCCGCCGCCAGAACACCACCACC AGAA-CCACCACCACCTGAAGAGACGGTGACC*; V<sub>L</sub> forward primer: *GGCGGC GGCGGCTCCGGTGGTGGTGGATCCGAAATGTGTTG-ACG CAGTC*; V<sub>L</sub> back primer: *GCGGCCGCTTGTATCTCCAC-CTTGGTCC*) and cloned by restriction digest into a bacterial expression vector slightly modified from pCANTAB5E (Amersham GE Healthcare). The resultant scFv 19G9 bacterial expression vector was used to create the diabody 19G9 expression vector. A PCR fragment generated using the V<sub>H</sub> forward and V<sub>L</sub> back primers was cloned into the TOPO Zero blunt sequencing vector (Invitrogen), and the following oligomers were used to create a 5–amino acid linker (GlyGlyGlyGlySer) between the V<sub>H</sub> and V<sub>L</sub> (oligomer 1: *CTTCAGGTGGTGGTG GTTCTGAAATTGTGTTG-ACGCAGTCTCC*; oligomer 2: *GGAGACTGCGTCAAC ACAATTTCAGAACACCACCACCTGAAG*) using the QuickChange site-directed mutagenesis kit (Stratagene). Finally, the NcoI/NotI fragment was ligated into the bacterial expression vector. Inserts and surrounding DNA were sequenced before transformation of vectors in *Escherichia coli* DH5α.

### Construction of the 19G9 Miniantibody Format

The IgE-C<sub>H</sub>4 dimerization domain was created by cloning the C<sub>H</sub>4 domain of IgE from commercial mRNA (clone 2132581; Invitrogen) using PCR primers (IgE-C<sub>H</sub>4 back primer: *CCGTC-AGTCTTCTCTTCCCCCGCGTGCTGCCCCGGAAG*; IgE-C<sub>H</sub>4 forward primer: *CGGATACGGCACCGGCGCACCTTACCGG-GATTT ACAGAC*). The IgG1 hinge region and the first β-strand of IgG1 C<sub>H</sub>2 was introduced by PCR (hinge primer: *TTCCTCT-TCCCCCGCGTGCTGCCCCG GAAG*). NotI and SgrA1 sites were introduced by primers (*CCGTCAGTCTTC CTCTTCCCCC-CGCGTGCTGCCCCGGAAG*) and (*CGGATACGGCACCGGCGCACCTTACCGGGATTACAGAC*), respectively. These sites permitted direct cloning into the single-chain bacterial expression vector (above). Four hydrophobic amino acids originally in the first β-strand of IgG1 C<sub>H</sub>2 (Val<sub>240</sub>PheLeuPhe<sub>243</sub>) were mutated to a hydrophilic tetrapeptide (AspSerGluTyr) using a DNA oligomer (*CAAAGCGCCGAGGGCGG GTGGTTCCACTCACACATG-CCCACCGTGCCAGCACCTGAACCTCTGGGGGGACCGTCA-GACAGCGAGTACCCCCCGCGTGCTGCCCCGGAAG*) and the QuickChange site-directed mutagenesis kits. The resultant miniantibody 19G9 construct was sequenced and ligated into a modified mammalian expression vector pKM for transfection into CHO K1 cells as described previously (8).

### Expression and Purification of Antibodies

The expression and purification of IgG 19G9 was described previously (2). The scFv 19G9 and diabody 19G9, both expressed in *E. coli* DH5α (7), and the miniantibody 19G9, expressed in Chinese hamster kidney (CHO) K1 cells (8), were expressed and purified by anti-E tag affinity chromatography using a purification module (RPAS; Amersham GE Healthcare), followed by size-

exclusion chromatography. The molecular weights of the purified antibodies (reduced and nonreduced) were confirmed by 4%–12% sodium dodecyl sulfate polyacrylamide gel electrophoresis (SDS-PAGE), which demonstrated formation of the disulfides in the hinge region of miniantibody 19G9 and insignificant contamination by the monomer (data not shown).

### Enzyme-Linked Immunosorbent Assay (ELISA)

Antigen binding by antibody fragments was measured by ELISA. Purified human mindin/RG-1 protein was immobilized on 96-well plates (Immobilon 4; Dynatech Laboratories, Inc.) in 0.1 M sodium bicarbonate, pH 9.5 (250 ng/well), overnight at 4°C. Wells were blocked 1 h with phosphate-buffered saline (PBS) containing 5 mg of bovine serum albumin (BSA) per milliliter and 0.05% polysorbate 20. Primary antibody dilutions (1:5 serial) from  $5 \times 10^{-7}$  M to  $1 \times 10^{-13}$  M were added, and plates were incubated for 2 h at room temperature. Wells were washed 3 times with buffer, and horseradish peroxidase (HRP)-labeled second antibody was added. HRP-goat antihuman IgG was used with IgG, and HRP-anti-E tag antibody was used for scFv, diabody, and miniantibody, which contain E-tag expression tags. After a 1-h incubation, plates were washed 4 times in buffer, and peroxidase substrate was added. After color development (~10 min), absorbance (405 nm) was measured using a Ultrospec II 96-well plate reader (LKB).

### Surface Plasmon Resonance (SPR) (Biacore)

Antibody affinity constants were determined by the Biacore method (Biacore International AB). Purified mindin/RG-1 was immobilized to the CM5 sensor chip (Amersham GE Healthcare) using standard amine coupling. Purified antibodies from 12.5 to 800 nM were bound to the surface using a Biacore 1000 instrument (Amersham GE Healthcare). Off-rates were determined by passing buffer over the bound antibody on the surface. Surfaces were regenerated with 250 mM glycine, pH 2.8. Kinetic constants were determined by fitting to a 1:1 Langmuir model using the instrument software.

### Generation of Antibody–Chelator Conjugates

All equipment was rendered metal-free with 10 mM ethylenediaminetetraacetic acid (EDTA) and extensive rinsing with Chelex-treated (BioRad) purified water. Buffers were prepared with reagents containing minimal trace metals and treated with Chelex resin to remove residual metals. Antibodies were concentrated to approximately 5 mg/mL by ultrafiltration, and EDTA was added to 1 mM for 1 h to remove bound trace metals. Buffer exchange into 50 mM sodium bicarbonate and 150 mM sodium chloride, pH 8.5, was performed using a size-exclusion column (SuperDex200; Pharmacia). Antibody-containing fractions were concentrated to between 5 and 10 mg/mL by ultrafiltration. A stock solution of CHX-A''-DTPA (Macrocyclics) prepared in anhydrous dimethylsulfoxide (100 mg/mL) was added to the antibody solution to a molar ratio of 50:1 (DTPA:Ab). The conjugation reaction was run overnight at room temperature. Unbound DTPA was removed from the reaction mixture by size-exclusion chromatography and the buffer exchanged to 50 mM sodium acetate and 150 mM NaCl, pH 6.5. Total protein concentration of the final immunoconjugate was determined by bicinchoninic acid assay (Pierce Biotechnology). The antigen binding by the immunoconjugates was determined by ELISA.

### Generation of Tumor-Bearing Mice

Naïve, athymic male nude (*nu/nu*) mice (Simonsen), aged 9–10 wk, were inoculated subcutaneously in the right hind flank with  $1 \times 10^7$  LNCaP (human prostate carcinoma) cells (ATCC) in a 1:1 suspension with Matrigel (BD). Animals bearing tumors less than 500 mm<sup>3</sup> by visual inspection at between 6 and 8 wk after cell inoculation were selected for biodistribution or PET studies. Mice were housed in facilities accredited by the American Association for Accreditation of Laboratory Animal Care, and all experiments were conducted in accordance with principles and procedures approved by the Animal Care and Use Committees at Berlex Biosciences and Washington University.

### <sup>111</sup>In Radiolabeling

Radiolabeling of the antibody–chelator conjugates with <sup>111</sup>In was performed via chelation of the radiometal to the DTPA moiety of the conjugate. <sup>111</sup>In-chloride (PerkinElmer Life Sciences, Inc.) was buffered with an equal volume of 100 mM sodium acetate, pH 5.5, and then the antibody–conjugate was added to a ratio of 37 MBq of antibody per milligram. The reaction continued for 1 h at room temperature with mixing and then was quenched with 1 mM EDTA to scavenge nonspecifically bound radioisotope while the reaction mix was incubated for an additional 15 min at room temperature. Radiolabeled antibody was separated from free radioisotope, and buffer exchanged into PBS, by size-exclusion chromatography. Antibody-containing fractions were collected and pooled.

Activity of the <sup>111</sup>In-radioconjugates was measured using a  $\gamma$ -counter (Packard Cobra II; GMI, Inc.). Total protein concentration was determined by bicinchoninic acid assay (Pierce Biotechnology), and specific activities were calculated on the basis of these results. Levels of free radioisotope and free DTPA were determined by thin-layer chromatography using a previously published method (9). The antigen-binding activity of the radioconjugate was measured by ELISA or radioimmunoassay.

### <sup>86</sup>Y Radiolabeling

<sup>86</sup>Y was produced using a published method (10). The constructs were labeled with <sup>86</sup>Y as previously reported (2). Briefly, 100  $\mu$ L of <sup>86</sup>Y-Cl<sub>3</sub> in 0.1 M hydrogen chloride was diluted with 300  $\mu$ L of 0.1 M ammonium acetate (pH 5.6), and 100- $\mu$ L aliquots (~18.5 MBq) were added to each antibody (500  $\mu$ g) and incubated at room temperature for 1 h. Then, 3  $\mu$ L of 0.5 M EDTA were added, and the reaction was incubated for 10 min. Reactions were loaded onto Biospin-6 columns (BioRad) preconditioned with PBS and centrifuged at 2,500 rpm for 4 min. Both the eluted labeled antibody and the free <sup>86</sup>Y retained in the column were counted to determine labeling efficiency.

### <sup>111</sup>In and <sup>86</sup>Y Acute Biodistribution Studies

The <sup>111</sup>In-labeled conjugates were injected (0.074 MBq/mouse) via the tail vein into LNCaP tumor-bearing mice. Animals were euthanized at 0.25, 3, 6, and 48 h after injection to determine levels of <sup>111</sup>In-labeled conjugates in the blood, tumor, liver, and kidney ( $n = 2$  per time point). Tissues were harvested and weighed before radioactivity content was determined in a  $\gamma$ -counter. Standards representing the injected dose per animal were used to calculate percentage injected dose per gram (%ID/g) of tissue and percentage injected dose per organ (%ID/organ).

The <sup>86</sup>Y-labeled conjugates were injected via the tail vein into LNCaP tumor-bearing nude mice (0.37 MBq/mouse). Animals

were euthanized at 4 h ( $n = 4$  per group) and 24 h ( $n = 5$  per group) after injection. At the 4-h time point, the tumor, blood, lung, liver, spleen, kidney, and skin were harvested. At the 24-h time point, the tumor, blood, lung, liver, spleen, kidney, muscle, fat, heart, brain, bone, testes, prostate, pancreas, skin, stomach, and intestines were harvested. All tissues were drained of blood, weighed, and counted in a  $\gamma$ -counter. By comparison with a standard representing the injected dose per animal, the samples were corrected for radioactive decay, to calculate %ID/g of tissue and %ID/organ.

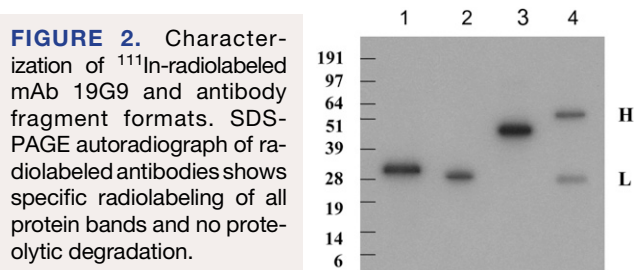
### <sup>86</sup>Y Small-Animal PET

All imaging was performed in a temperature-controlled imaging suite with close monitoring of the physiologic status of the animals. Imaging was performed between 0 and 1 h and at 4, 24, 48, and 72 h after injection (2.96 MBq/mouse, intravenously). Small-animal PET was performed using the microPET Focus-120 or -220 system (Concorde Microsystems Inc.) (11). The small-animal PET images were coregistered in combination with a micro-CT-II camera (Imtek Inc.), which provides high-resolution CT anatomic images at selected time points with selected constructs. CT and PET images were registered using the landmark AMIRA image-display software (TGS Inc.). The registration method consisted of rigid transformation of the CT images from landmarks provided by fiducial markers directly attached to the animal bed. Time-activity curves were generated from regions of interest drawn to encompass the entire tumor and other organs of interest.

## RESULTS

### Characterization of Antibodies and Conjugates

All parental bivalent antibody formats had comparable affinities, with affinity constant ( $K_D$ ) values measured in the low nanomolar range, as determined by SPR (Table 1). The monovalent scFv format had a 10-fold lower  $K_D$  due to its lower avidity. After the antibody-chelator immunoconjugates were synthesized and subsequently radiolabeled, the proteins were characterized by electrophoresis and autoradiography of the <sup>111</sup>In-labeled antibodies on SDS-PAGE. Under reducing conditions, both light and heavy chains of the IgG and the single chains of the other antibody fragment formats were radiolabeled with no evidence of degradation (Fig. 2). More than 98% of the radioactivity was localized to the antibody as determined by thin-layer chromatography, and levels of free <sup>111</sup>In-DTPA and free <sup>111</sup>In were minimal (Table 2). The antigen-binding activity of the labeled antibodies was verified by solid-phase radioimmunoassay and ELISA (data not shown). Thus, the radiolabeled antibodies administered in vivo retained their antigen specificity and were of high quality, with excellent radiochemical purity. The specific activities for <sup>111</sup>In-IgG,



<sup>111</sup>In-mini-antibody, and <sup>111</sup>In-diabody were 17.8, 85.5, and 19.6 MBq/mg, respectively. The specific activity of the <sup>111</sup>In-scFv could not be determined accurately because of a low protein concentration in the labeling reaction. After these CHX-A''-DTPA-immunoconjugates were radiolabeled with <sup>86</sup>Y, specific activities of 29.6, 31.8, 30.21, and 39.6 MBq/mg were achieved for the IgG, scFv, diabody, and mini-antibody, respectively. The radiolabeling efficiency was high, ranging from between 82% and 96%.

### <sup>111</sup>In Biodistribution

The <sup>111</sup>In-antimindin/RG-1 antibody construct accumulation in the blood, tumor, liver, and kidney of mice bearing subcutaneous LNCaP tumors was determined from %ID/g values (Table 3; Fig. 3). Clearance rates from the blood were inversely correlated with molecular size of the construct: scFv > diabody > mini-antibody > IgG. Smaller constructs were rapidly eliminated by renal clearance, especially the scFv (25 kDa) and diabody (50 kDa), which are both smaller than the renal clearance threshold of approximately 65 kDa. Early accumulation of the constructs in the kidneys, in descending order, was diabody > scFv > mini-antibody > IgG (at 6 h:  $90.4 \pm 4.1$  %ID/g for the diabody,  $29.2 \pm 0.2$  %ID/g for the scFv,  $12.1 \pm 0.01$  %ID/g for the mini-antibody, and  $4.6 \pm 0.8$  %ID/g for the IgG). The scFv levels in the kidney were lower than those of the larger diabody construct because, by the initial time point (15 min), much of the scFv had already been cleared. The scFv kidney levels decrease over time, compared with the diabody levels, which increase to a maximum at 3 h and then decrease. Liver accumulation was comparable for the IgG and mini-antibody constructs and lower for the diabody and scFv constructs. Rapid renal clearance may preclude accumulation of the smaller constructs in the liver and other tissues including tumor. At 48 h, the tumor accumulation of

**TABLE 1.** Kinetic Constants of 19G9 IgG Antibody and Fragment Antibody Formats Measured by SPR

Antibody format	Constant			
	$k_a$ (1/mol s)	$k_d$ (1/s)	$K_A$ (1/M)	$K_D$ (M)
scFv 19G9	$9.0 \times 10^4$	$1.7 \times 10^{-3}$	$5.3 \times 10^7$	$1.9 \times 10^{-8}$
Diabody 19G9	$1.85 \times 10^5$	$2.14 \times 10^{-4}$	$9.0 \times 10^8$	$1.2 \times 10^{-9}$
Mini-antibody 19G9	$7.6 \times 10^5$	$1.14 \times 10^{-4}$	$6.7 \times 10^8$	$2.0 \times 10^{-9}$
IgG 19G9	$1.1 \times 10^5$	$1.1 \times 10^{-4}$	$9.9 \times 10^8$	$1.2 \times 10^{-9}$

Antibody format	<sup>111</sup> In-Antibody	<sup>111</sup> In-CHX-A''-DTPA	Free <sup>111</sup> In
scFv 19G9	98.20%	0.49%	1.31%
Diabody 19G9	99.72%	0.12%	0.16%
Miniantibody 19G9	99.10%	0.70%	0.29%
IgG 19G9	99.79%	0.08%	0.13%

Values are based on percentage of total counts in 1- $\mu$ L sample as free <sup>111</sup>In, free radiolabeled DTPA, and radiolabeled antibody.

the labeled IgG and miniantibody was greater than that of the diabody or scFv formats ( $24.1 \pm 1.2$  %ID/g for the IgG,  $14.2 \pm 1.8$  %ID/g for the miniantibody,  $2.4 \pm 0.3$  %ID/g for the diabody, and  $0.4 \pm 0.1$  %ID/g for the scFv).

The kinetics of tumor uptake over 48 h with the four <sup>111</sup>In-19G9 antibody formats in LNCaP tumor-bearing mice is illustrated in Figure 4. The IgG format showed continuous accumulation of antibody, reaching 24.1 %ID/g at 48 h. The miniantibody format also accumulated in the tumor, to reach a lower maximum of 14.2 %ID/g after 48 h. The maximum diabody accumulation of 3.7 %ID/g occurred after only 3 h, and the scFv did not attain measurable deposition in the tumors at any time.

#### **<sup>86</sup>Y Biodistribution**

The accumulation of <sup>86</sup>Y-antimindin/RG-1 antibody constructs as determined from %ID/g was measured in 17 different tissues 24 h after intravenous injection and in 7 tissues 4 h after administration. Significant accumulation (>6 %ID/g) of antibody was observed in 4 tissues tested (blood, tumor, liver, and kidney) (Table 4; Fig. 5). Accumulation results for all tissues are in Supplemental Table 1 (supplemental materials are available online only at <http://jnm.snmjournals.org>).

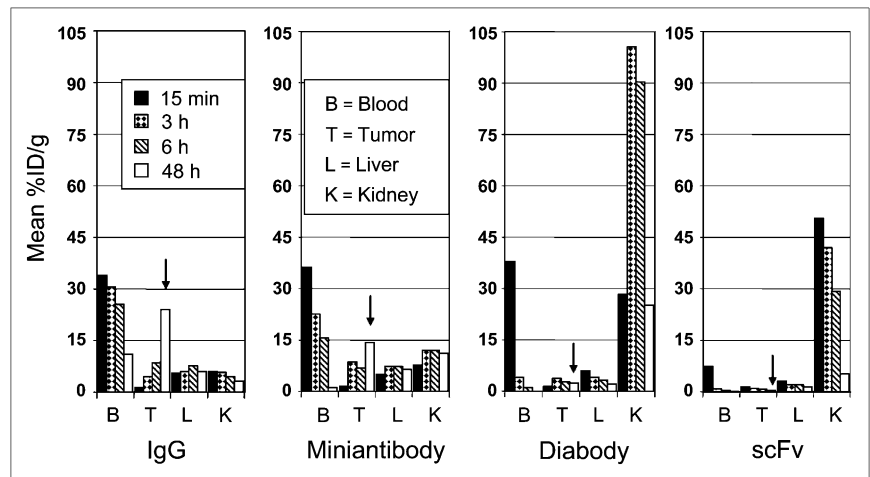
Antibody localization to the tumor at 24 h after injection was proportional to molecular size, with IgG > miniantibody > diabody > scFv ( $20.2 \pm 2.0$  %ID/g for the IgG,  $13.1 \pm 3.6$  %ID/g for the miniantibody,  $3.7 \pm 0.8$  %ID/g for the diabody, and  $0.54 \pm 0.13$  %ID/g for the scFv). Circulating antibody levels in the blood at 24 h were also proportional to molecular size ( $15.9 \pm 4.0$  %ID/g for IgG,  $4.0 \pm 0.9$  %ID/g for the miniantibody,  $0.1 \pm 0.04$  %ID/g for the diabody, and  $0.04 \pm 0.04$  %ID/g for the scFv). The scFv and diabody formats were rapidly cleared by the kidneys. As early as 4 h after injection, the scFv was nearly completely eliminated from the blood, leaving insufficient time for accumulation in the tumor. In contrast, the IgG and miniantibody formats remained at higher concentrations in the blood, allowing for higher accumulation in the tumor by 24 h. Accumulation of the different antibody formats in the kidney is transient, reflecting renal clearance activities.

Overall, the results of the <sup>111</sup>In biodistribution study show strong similarity to results of the <sup>86</sup>Y biodistribution study. Both studies show longer residence times of the IgG and miniantibody in the blood and correspondingly higher tumor accumulation in the tumor, compared with the scFv and diabody. Nearly complete elimination of the diabody from the blood was achieved by 3 h, and peak kidney levels

Antibody format	Time (h)	Tissue			
		Blood	Tumor	Liver	Kidney
IgG	0.25	33.9 (2.4)	1.3 (0.4)	5.6 (2.1)	6.0 (2.4)
	3	30.6 (6.3)	4.5 (0.2)	6.0 (1.6)	5.8 (1.6)
	6	25.6 (2.7)	8.7 (1.4)	7.6 (1.9)	4.6 (0.8)
	48	11.0 (1.4)	24.1 (1.2)	6.1 (0.1)	3.2 (0.1)
Miniantibody	0.25	36.2 (6.4)	1.6 (0.3)	5.0 (0.9)	7.6 (1.0)
	3	22.5 (3.0)	8.6 (4.6)	7.3 (1.3)	11.9 (0.6)
	6	14.1 (1.4)	6.9 (0.5)	7.3 (0.9)	12.1 (0.01)
	48	1.1 (0.2)	14.2 (1.8)	6.5 (0.3)	11.2 (1.6)
Diabody	0.25	37.8 (5.4)	1.4 (0.5)	5.9 (1.0)	28.2 (8.3)
	3	3.9 (0.2)	3.7 (1.4)	4.0 (1.3)	101 (28)
	6	1.1 (0.2)	2.7 (0.7)	3.3 (0.7)	90.4 (4.1)
	48	0.03 (0.0)	2.4 (0.3)	2.1 (0.2)	25.1 (2.0)
scFv	0.25	7.3 (0.7)	1.5 (0.2)	3.1 (0.2)	50.5 (3.4)
	3	0.9 (0.1)	1.0 (0.03)	2.1 (0.8)	41.9 (3.5)
	6	0.4 (0.01)	0.7 (0.01)	2.0 (0.1)	29.2 (0.2)
	48	0.04 (0.01)	0.4 (0.1)	1.4 (0.4)	5.2 (0.5)

Results are percentage of initial dose recovered in each tissue (average %ID/g), with SD in parentheses.

**FIGURE 3.** Biodistribution of  $^{111}\text{In}$ -antibodies in LNCaP tumor-bearing mice showing  $^{111}\text{In}$  accumulation at 0.25, 3, 6, and 48 h after injection in blood, tumor, liver, and kidney. Values are mean %ID/g of tissue. Arrows indicate accumulation in tumor at 48 h.



of the diabody were detected at 3 and 4 h in the  $^{86}\text{Y}$  and  $^{111}\text{In}$  studies, respectively, with tumor accumulation less than 3 %ID/g at 24 and 48 h. Elimination of the scFv from the blood was even more rapid, with 95% clearance of the  $^{111}\text{In}$  labeled scFv by 15 min. Kidney levels of the scFv were lower than those of the diabody; however, the declining levels from 15 min suggest that peak levels were reached before 15 min. This finding is consistent with the low levels seen in the blood at the early time points and indicates rapid renal clearance rates for the scFv. Blood clearance, tumor accumulation, renal clearance, and liver accumulation were all similar when antibody fragments were labeled with  $^{111}\text{In}$  or  $^{86}\text{Y}$ .

#### $^{86}\text{Y}$ Small-Animal PET

Small-animal PET provided an additional method to determine in vivo tissue biodistribution and tumor localization of the  $^{86}\text{Y}$ -labeled IgG and antibody fragment formats. Figure 6A illustrates tumor accumulation of the 4

antibody formats, 48 h after administration. Significant accumulation in tumors was seen with 3 conjugates: IgG, mini-antibody, and diabody. The scFv was not detected in tumors by PET. In mice receiving IgG, significant accumulation was localized in the tumor. Antibody not yet cleared from circulation is also apparent, particularly in the heart. Residual kidney accumulation and no tumor uptake were visible in mice receiving scFv. In addition to accumulation in the tumor, diabody and mini-antibody were detected in the kidney and liver. Mini-antibody was also detectable in the blood at 48 h. An imaging time course (0 to 1 and 4, 24, 48, and 72 h after injection) suggests all fragments except the IgG underwent renal clearance of varying degrees and that accumulation in the tumor became discernable between 4 and 24 h after injection (Figs. 6B and 6C). The PET results are consistent with the results of the  $^{111}\text{In}$  and  $^{86}\text{Y}$  biodistribution studies.

Combined CT and PET, compared with CT or PET alone, at 48 h after injection produced enhanced anatomic identification of  $^{86}\text{Y}$  localization in tumor-bearing mice (Fig. 7). Accumulation of the IgG (Fig. 7A) within the tumor, located near the rear femur, is clearly visible, as is IgG present in the liver and intraperitoneal blood. In comparison, scFv is only detectable in the kidney and not in the tumor, blood, or other organs.

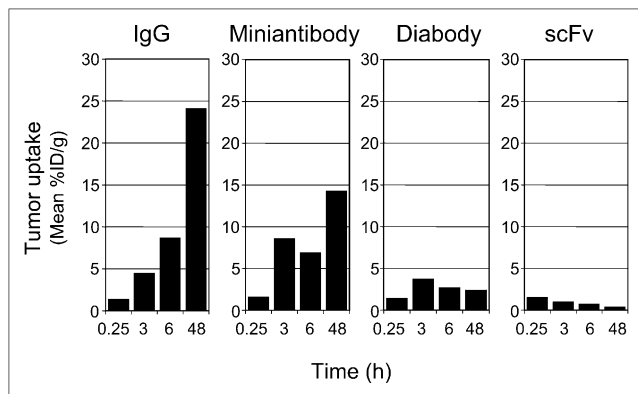


**FIGURE 4.** Tumor uptake of  $^{111}\text{In}$ -19G9 antibodies in LNCaP tumor xenografts in nude mice. Values represent mean %ID/g of tumor tissue at 0.25, 3, 6, and 48 h after injection.

#### DISCUSSION

The 19G9 IgG antibody was previously demonstrated to be a promising format for  $^{90}\text{Y}$  radioimmunotherapy and  $^{86}\text{Y}$  PET of mindin/RG-1-expressing tumors, after conjugation with CHX-A''-DTPA and radiolabeling (2). Here, we compare the biodistribution and PET properties of 4 matched antibody formats of the 19G9 antibody, all of which are potent binders of mindin/RG-1, after conjugation by CHX-A''-DTPA. Interest continues in the development of alternative antibody formats to improve the clinical performance of therapeutic and diagnostic antibodies

**TABLE 4.** Biodistribution of  $^{86}\text{Y}$ -Labeled Antibody Formats in LNCaP Tumor-Bearing Male *nu/nu* Mice

Antibody format	Time (h)	Tissue			
		Blood	Tumor	Liver	Kidney
IgG	4	18.4 (1.8)	1.8 (0.5)	5.3 (1.3)	3.8 (0.6)
	24	15.9 (4.0)	20.2 (2.0)	5.2 (1.0)	3.7 (0.7)
Miniantibody	4	6.7 (1.2)	0.8 (0.3)	4.4 (0.9)	4.9 (1.2)
	24	4.0 (0.9)	13.1 (3.6)	11.0 (3.7)	11.1 (2.5)
Diabody	4	2.1 (0.6)	1.5 (0.3)	3.9 (0.6)	64.1 (13.2)
	24	0.1 (0.04)	3.7 (0.8)	4.7 (1.1)	51.5 (9.4)
scFv	4	0.23 (0.05)	0.29 (0.04)	0.53 (0.16)	21.4 (5.5)
	24	0.04 (0.04)	0.54 (0.13)	0.57 (0.1)	11.8 (3.7)

Results are percentage of initial dose recovered in each tissue (average %ID/g), with SD in parentheses.

(3,6,12). Development of a single optimized format coupled to a chelator capable of binding a variety of radiometals, such as  $^{90}\text{Y}$  for therapy or  $^{86}\text{Y}$  for imaging or dosimetry measurement, may be useful in multiple clinical applications.

The size of the construct profoundly affects the biokinetics of each agent. The smallest construct (scFv) was rapidly and efficiently extracted from the blood and removed, primarily via the renal system, before significant tumor accumulation. In contrast, the largest construct (IgG) demonstrated prolonged blood retention and significant tumor uptake. Although deposition of  $^{111}\text{In}$ -IgG in the tumor was detected as early as 3 h after administration, the tumor-to-blood ratio (%ID/g) did not exceed 1.0 until between 6 and 48 h. PET detected IgG tumor deposition at 24 h. The diabody and miniantibody fragments both demonstrated intermediate blood clearance and tumor localization. Diabody blood levels were rapidly reduced during the initial hours, and tumor deposition was probably not sufficient for radiotherapy. High kidney levels were found for the diabody at 3 and 6 h. PET of the diabody at 48 h did, however, show comparable tumor delineation to that of the IgG and miniantibody.

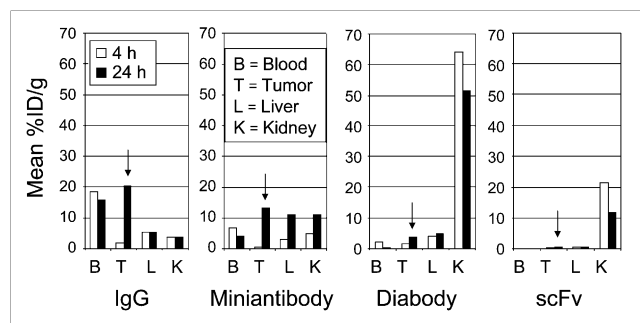


**FIGURE 5.** Biodistribution results of  $^{86}\text{Y}$ -antibodies in LNCaP tumor-bearing mice showing  $^{86}\text{Y}$  accumulation at 4 h (white) and 24 h (black) in blood, tumor, liver, and kidney. Values are mean %ID/g of tissue. Arrows indicate accumulation in tumor at 24 h.

Which construct is most suitable for imaging or therapy or both? Three constructs—IgG, diabody, and miniantibody—all delineate the tumor volume within 24 h. However, it is clear from the time course (Fig. 6) that labeled miniantibody delineates the tumor within 4 h of administration (aided by a low background resulting from the rapid blood clearance), suggesting that the miniantibody should be studied further in imaging applications.

The data show that the IgG construct has higher overall accumulation within the tumor at both 4 and 24 h for  $^{86}\text{Y}$  and at 48 h for the  $^{111}\text{In}$  analog. This effect, combined with reduced nontarget organ uptake at 24 h, may result in better therapeutic efficacy from  $^{90}\text{Y}$ -IgG treatment. Possible radiologic toxicity, especially to radiosensitive tissues such as bone marrow, resulting from prolonged circulation, must be minimized by careful dosimetry. PET, using the same antibody-chelator construct labeled with  $^{86}\text{Y}$ , might be feasible for predicting  $^{90}\text{Y}$  dosimetry. By fine-tuning the molecular size of these biomolecules, it is possible to generate agents that have potential as either imaging or therapeutic radiopharmaceuticals.

In a previous study, the biodistribution of 3 dimeric antibody formats was compared using an antibody (L19) that specifically targeted the extra domain B(ED-B) of fibronectin localized to the tumor vasculature (13). The  $^{125}\text{I}$ -radiolabeled 80-kDa small immunoprotein format of the anti-ED-B antibody, similar in size to the miniantibody, achieved the highest tumor-to-blood ratio, when compared with the diabody and IgG. In a subsequent study, the  $^{99\text{m}}\text{Tc}$ -radiolabeled diabody format of the L19 antibody was shown to efficiently allow scintigraphic imaging of F9 tetracarcinoma tumors in mice (14). In practice, PET compares favorably with conventional imaging techniques. In this study we directly compared the biodistribution and PET properties of 4 antibody formats derived from the same antibody: the monomeric scFv, dimeric diabody, miniantibody, and IgG formats.

Molecular weight differences between antibody formats will influence clearance by the kidneys. However, in the case of the IgG format, the presence of the Fc domain leads to further considerations because of Fc receptor binding. Mutagenesis studies of the Fc region of IgG (15) allow

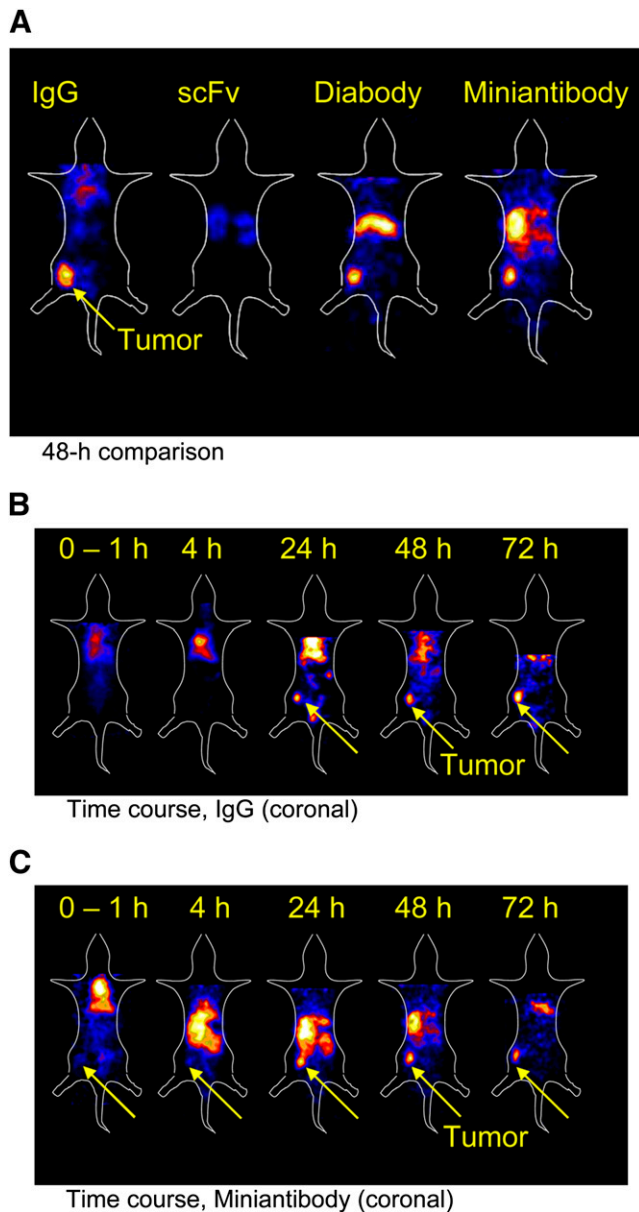


**FIGURE 6.** PET (coronal) of  $^{86}\text{Y}$ -labeled 19G9 in mice implanted with subcutaneous LNCaP tumors. (A) Comparison of 4 antibody constructs (IgG, scFv, diabody, and mini-antibody) at 48 h, illustrating relative tumor localization of antibodies. Time course showing localization of  $^{86}\text{Y}$ -IgG (B) and  $^{86}\text{Y}$ -mini-antibody (C) at 5 time points between 0 and 72 h after injection. Arrows indicate tumor.

selection of Fc functionalities in the IgG such as enhanced complement activation via C1q binding (16), improved ability to activate immune cells, antibody-dependent cellular cytotoxicity and other mechanisms dependent on binding to various Fc $\gamma$ Rs (17,18), and enhanced clearance properties based on modifications to optimize FcRn interactions (19–21). Although formats such as the scFv, diabody, and mini-antibody will not benefit from extended serum half-lives provided by FcRn binding, they will not trigger these other biologic functions mediated by the Fc.

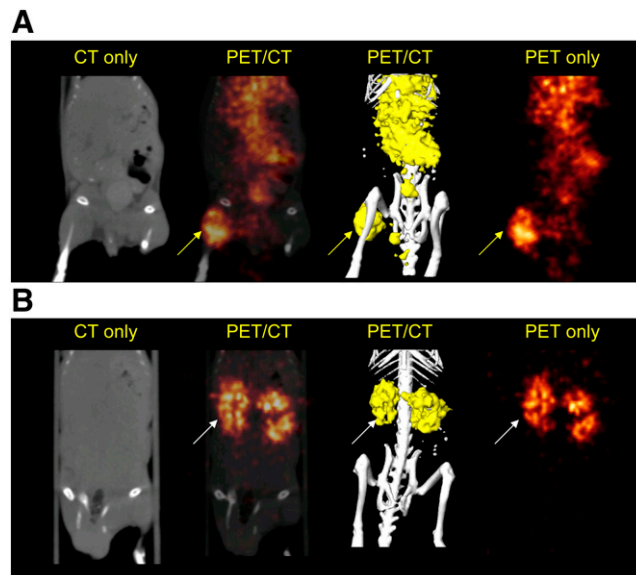


**FIGURE 7.** PET/CT (coronal) image at 48 h in mice implanted with subcutaneous LNCaP tumors using either  $^{86}\text{Y}$ -labeled IgG (A) or  $^{86}\text{Y}$ -labeled scFv (B). Yellow arrows indicate accumulation in tumor, and white arrows indicate accumulation in kidney.

The potency of monomeric and dimeric formats differs because of the avidity effect. Dimeric constructs bind with higher affinity than do monomeric constructs. However, there is an emerging recognition that potent binding molecules may not be the best therapeutic antibodies (22) or therapeutic biologics (23), because high-affinity binding may inhibit tissue penetration or lead to more rapid degradation and clearance. Engineering both valency and affinity for optimal in vivo tumor distribution was demonstrated using a series of radiolabeled scFvs and diabodies of varying potency targeting the cell surface tumor marker c-erbB-2 on SK-OV-3 human tumor xenografts (24). In contrast to the latter study, the present work compares antibody molecules that differ only in molecular size, while retaining the identical binding affinities for the 3 dimeric formats (Table 1).

## CONCLUSION

These data show that one of these new constructs could be developed as either  $^{111}\text{In}$ -SPECT or  $^{86}\text{Y}$ -PET radiopharmaceuticals. Moreover, the use of the imaging/therapy pair  $^{86}\text{Y}/^{90}\text{Y}$  with the most suitable therapeutic construct will allow researchers to accurately determine the localization of the therapeutic agents and to determine individualized patient dosimetry.

## ACKNOWLEDGMENTS

We are grateful to Terry Sharp, Lori Strong, Nicole Fettig, Margaret Morris, Amanda Roth, Ann Stroncek, and John McClary for expert technical assistance. We also thank Kathy White and Jerrel Rutlin for animal handling and PET imaging

support; Ron Cobb, Andrezej Citkowics, and Brent Larsen for production and purification of antibodies; and Susan Adams for cell preparation. Dr. Martin W. Brechbiel, National Cancer Institute, Bethesda, Maryland, provided helpful discussions. Thanks also to the Cancer Research Department of Berlex Biosciences and Schering AG for financial support.

## REFERENCES

1. Feinstein Y, Klar A. The neuronal class 2 TSR proteins F-spondin and mindin: a small family with divergent biological activities. *Int J Biochem Cell Biol.* 2004;36:975–980.
2. Parry R, Schneider D, Hudson D, et al. Identification of a novel prostate tumor target, mindin/RG-1, for antibody-based radiotherapy of prostate cancer. *Cancer Res.* 2005;65:8397–8405.
3. Holliger P, Hudson PJ. Engineered antibody fragments and the rise of single domains. *Nat Biotechnol.* 2005;23:1126–1136.
4. Hu S, Shively L, Raubitschek A, et al. Minibody: a novel engineered anti-carcinoembryonic antigen antibody fragment (single-chain Fv-CH3) which exhibits rapid, high-level targeting of xenografts. *Cancer Res.* 1996;56:3055–3061.
5. Lindner P, Plueckthun A. Miniantibodies. In: Kontermann R, Duebel S, eds. *Antibody Engineering*. Berlin, Germany: Springer Verlag; 2001:637–647.
6. Hagemeyer CE, Schwarz M, Peter K. Single-chain antibodies as new antithrombotic drugs. *Semin Thromb Hemost.* 2007;33:185–195.
7. Heitner T, Satozawa N, McLean K, et al. Obligate multivalent recognition of cell surface tomoregulin following selection from a multivalent phage antibody library. *J Biomol Screen.* 2006;11:985–995.
8. Xia W, Bringmann P, McClary J, et al. High levels of protein expression using different mammalian CMV promoters in several cell lines. *Protein Expr Purif.* 2006;45:115–124.
9. Nikula TK, Curcio MJ, Brechbiel MW, Gansow OA, Finn RD, Scheinberg DA. A rapid single vessel method for preparation of clinical grade ligand conjugated monoclonal antibodies. *Nucl Med Biol.* 1995;22:387–390.
10. Yoo J, Tang L, Perkins TA, et al. Preparation of high specific activity  $^{86}\text{Y}$  using a small biomedical cyclotron. *Nucl Med Biol.* 2005;32:891–897.
11. Tai YC, Ruangma A, Rowland DJ, et al. Performance evaluation of the microPET focus: a third-generation microPET scanner dedicated to animal imaging. *J Nucl Med.* 2005;46:455–463.
12. Albrecht H, DeNardo SJ. Recombinant antibodies: from the laboratory to the clinic. *Cancer Biother Radiopharm.* 2006;21:285–304.
13. Borsi L, Balza E, Bestagno M, et al. Selective targeting of tumoral vasculature: comparison of different formats of an antibody (L19) to the ED-B domain of fibronectin. *Int J Cancer.* 2002;102:75–85.
14. Berndorff D, Borkowski S, Moosmayer D, et al. Imaging of tumor angiogenesis using  $^{99\text{m}}\text{Tc}$ -labeled human recombinant anti-ED-B fibronectin antibody fragments. *J Nucl Med.* 2006;47:1707–1716.
15. Shields RL, Namenuk AK, Hong K, et al. High resolution mapping of the binding site on human IgG1 for Fc $\gamma$ RI, Fc $\gamma$ RII, Fc $\gamma$ RIII, and FcRn and design of IgG1 variants with improved binding to the Fc $\gamma$ R. *J Biol Chem.* 2001;276:6591–6604.
16. Idusogie EE, Wong PY, Presta LG, et al. Engineered antibodies with increased activity to recruit complement. *J Immunol.* 2001;166:2571–2575.
17. Woof JM. Immunology: tipping the scales toward more effective antibodies. *Science.* 2005;310:1442–1443.
18. Carter P. Improving the efficacy of antibody-based cancer therapies. *Nat Rev Cancer.* 2001;1:118–129.
19. Petkova SB, Akilesh S, Sproule TJ, et al. Enhanced half-life of genetically engineered human IgG1 antibodies in a humanized FcRn mouse model: potential application in humorally mediated autoimmune disease. *Int Immunol.* 2006;18:1759–1769.
20. Olafsen T, Kenanova VE, Wu AM. Tunable pharmacokinetics: modifying the in vivo half-life of antibodies by directed mutagenesis of the Fc fragment. *Nat Protocols.* 2006;1:2048–2060.
21. Datta-Mannan A, Witcher DR, Tang Y, Watkins J, Wroblewski VJ. Monoclonal antibody clearance: impact of modulating the interaction of IgG with the neonatal Fc receptor. *J Biol Chem.* 2007;282:1709–1717.
22. Weiner LM, Carter P. Tunable antibodies. *Nat Biotechnol.* 2005;23:556–557.
23. Sarkar CA, Lowenhaupt K, Horan T, Boone TC, Tidor B, Lauffenburger DA. Rational cytokine design for increased lifetime and enhanced potency using pH-activated “histidine switching.” *Nat Biotechnol.* 2002;20:908–913.
24. Adams GP, Tai MS, McCartney JE, et al. Avidity-mediated enhancement of in vivo tumor targeting by single-chain Fv dimers. *Clin Cancer Res.* 2006;12:1599–1605.